

RECONSTRUCTION OF TIME-VARYING FIELDS IN WIRELESS SENSOR NETWORKS USING SHIFT-INVARIANT SPACES: ITERATIVE ALGORITHMS AND IMPACT OF SENSOR LOCALIZATION ERRORS

Günter Reise and Gerald Matz

Institute of Communications and Radio-Frequency Engineering, Vienna University of Technology
Gussibusstrasse 25/389, 1040 Vienna, Austria; email: {greise, gmatz}@nt.tuwien.ac.at

ABSTRACT

Based on the concept of hybrid shift-invariant spaces, we develop a distributed protocol for the reconstruction of time-varying physical fields in wireless sensor networks. The localized nature of these spaces allows for a clustered network architecture that leads to low communication overhead. Capitalizing on the sparsity of the reconstruction matrix, we propose an iterative reconstruction algorithm whose complexity per time-slot is linear in the number of sensors. We furthermore analyse the impact of sensor localization errors on the mean square error of the reconstructed field and provide numerical simulations illustrating our results.

Index Terms— Wireless sensor network, field reconstruction, shift-invariant space, B-splines

1. INTRODUCTION

Wireless sensor networks (WSN) are used for numerous monitoring tasks using remote sensors that are deployed over a region to be monitored in order to measure, process, and communicate information about a physical quantity of interest. In this paper, we build on our previous work [1, 2] dealing with the reconstruction of a physical field using a clustered WSN and the theory of shift-invariant spaces [3]. Such signal spaces entail extremely low computational complexity and match physical reality better than the band-limited (BL) spaces considered previously (e.g. [4, 5]). BL spaces are problematic since the spatial sampling performed by the WSN cannot be preceded by an anti-aliasing filter and strong oversampling may be required to achieve small reconstruction errors when dealing with non-BL fields [6].

The novel aspects in this paper compared to [1, 2] are:

- We extend our method to be applicable to *time-varying* fields. Rather than using direct solvers for the underlying system of equations as in [1, 2], we propose to apply iterative solvers that can be initialized with the solution obtained in the previous time step, thereby further reducing the computational complexity.
- We provide analytic and numerical investigations of the impact of sensor localization errors on the performance of our field reconstruction method. It turns out that shift-invariant interpolation is much more robust to localization errors than BL interpolation.

We have shown in [1, 2] that our clustered approach requires only local communication (one transmission to the cluster-head per sensor per time-slot) and has a complexity that scales linearly with the

number of sensors. For these reasons, there is no need to consider fully distributed architectures like e.g. [7] where the sensor repeatedly exchange intermediate results to split the computational complexity more evenly across sensors at the expense of increased communication overhead.

The rest of the paper is organized as follows. In Section 2 we describe the architecture of the WSN. The field model based on hybrid shift-invariant spaces and their underlying generators are discussed in Section 3. In Section 4, we outline our general approach and efficient implementations for reconstructing time-varying fields. The influence of sensor localization errors on the reconstruction quality is analysed in Section 5. Simulation results are shown in Section 6 and conclusions are provided in Section 7.

2. CLUSTERED WSN

We consider a WSN consisting of I sensors (nodes) that are deployed over a region \mathcal{A} in order to monitor a two-dimensional (2-D) time-varying physical field $h(x, y; t)$ (here, x and y denote the spatial coordinates and t denotes time). The position of sensor i is given by (x_i, y_i) and its measurements read $h_i(n) = h(x_i, y_i; nT)$ with T denoting the sampling period.

The sensors are grouped into M clusters \mathcal{C}_m of size I_m , $m = 1, \dots, M$, with each cluster monitoring a subregion \mathcal{A}_m such that $\bigcup_{m=1}^M \mathcal{A}_m = \mathcal{A}$ (see Fig. 1 for an example with $M = 4$). For simplicity, we assume in the following that the subregions \mathcal{A}_m are disjoint. In case the \mathcal{A}_m are not disjoint, our method can be modified suitably to average the field reconstruction results in the overlapping regions. In each cluster \mathcal{C}_m there is one node, termed the “cluster-head”, which collects the measurements $h_i(n)$ and the positions (x_i, y_i) of all nodes in the cluster and uses this information to reconstruct the field $h(x, y; t)$, $(x, y) \in \mathcal{A}_m$. This requires that each sensor determines its own position, which can be accomplished using the localization techniques summarized e.g. in [8]. We note that the clustered architecture that limits all communication and computation tasks to the individual clusters without any effect on the respective other clusters is suggested and enabled by the localized nature of the shift-invariant spaces used to model the physical field. It also permits a local adaptation of the field model (see Section 3.1) and avoids that a poor field reconstruction quality within a given cluster \mathcal{C}_m degrades the reconstruction of $h(x, y; t)$ within $\mathcal{A} \setminus \mathcal{A}_m$.

3. FIELD MODEL

3.1. Hybrid Shift-Invariant Spaces

Our reconstruction algorithm is based on modeling the considered fields via *hybrid shift-invariant spaces*. These spaces, first consid-

Funded by FWF Grant N10606 and WWTF Grant ICT08-044.

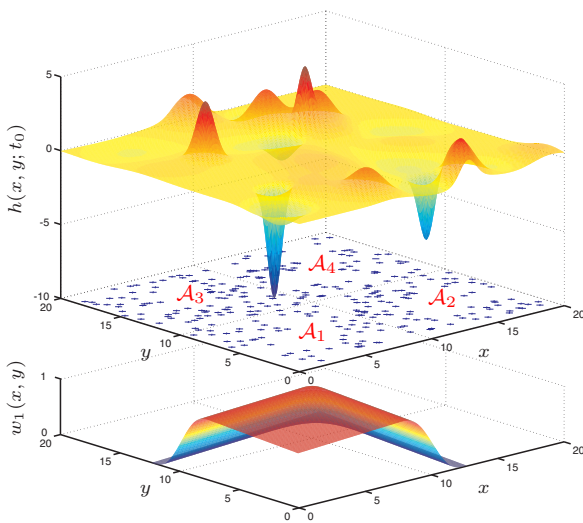


Fig. 1. Illustration of a WSN with four clusters monitoring a diffusion field $h(x, y; t)$; the weight function $w_1(x, y)$ is used for reconstruction within the cluster \mathcal{A}_1

ered in [2], extend ordinary shift-invariant spaces [3, 9] by using multiple generator functions. Consider a partition of \mathbb{Z}^2 into disjoint sets \mathbb{A}_m , $m = 1, \dots, M$, i.e., $\mathbb{Z}^2 = \bigcup_{m=1}^M \mathbb{A}_m$, $\mathbb{A}_m \cap \mathbb{A}_l = \emptyset$, $m \neq l$. To each subset \mathbb{A}_m , we associate a square-integrable generator function $g_m(x, y)$. In the context of our WSN, we choose $\mathbb{A}_m = \mathcal{A}_m \cap \mathbb{Z}^2$. The corresponding hybrid shift-invariant space is then defined as the linear subspace that comprises all weighted superpositions of spatial translates of the generator functions $g_m(x, y)$:

$$V(\mathcal{G}) = \left\{ f(x, y) : f(x, y) = \sum_{m=1}^M \sum_{(k,l) \in \mathbb{A}_m} c_{k,l} g_m(x-k, y-l) \right\}, \quad (1)$$

where $\mathcal{G} = \{g_m(x, y)\}_{m=1, \dots, M}$ and $c_{k,l}$ are square-summable coefficients. To guarantee the stability of (1), we assume that the set $\bigcup_{m=1}^M \{g_m(x-k, y-l)\}_{(k,l) \in \mathbb{A}_m}$ forms a Riesz basis for $V(\mathcal{G})$ [3]. Using different generator functions $g_m(x, y)$ for the sets \mathbb{A}_m allows to locally adapt the smoothness properties of the functions in $V(\mathcal{G})$. Conventional shift-invariant spaces are re-obtained as special case with identical generators, i.e., $g_1(x, y) = g_2(x, y) = \dots = g_M(x, y)$.

For the time-varying fields considered in this paper, we will assume that $h(x, y; t) \in V(\mathcal{G})$ for all time instants t . Since we keep the generator functions constant over time, this means that the field coefficients in (1) become time-dependent. Even though we do not impose an explicit mathematical model on the coefficients $c_{k,l}(t)$, we will implicitly rely on their rate of time variation being small.

3.2. Compactly Supported Generator Functions

In order to enable local field reconstruction with low complexity, we restrict ourselves to compactly supported generator functions, i.e. $g_m(x, y) = 0$ for $(x, y) \notin [-S_m/2, S_m/2] \times [-S_m/2, S_m/2]$.

Particularly convenient generator functions with compact support are basis-splines (B-splines), which have minimal support with respect to a given degree. Specifically, in the remainder of this paper we will restrict the choice of generator functions to 2-D B-spline functions which are constructed as $b_n(x, y) = \tilde{b}_n(x)\tilde{b}_n(y)$. Here, the one-dimensional cardinal B-splines of order n are defined via the

n -fold convolution

$$\tilde{b}_n(x) \triangleq \Pi(x) * \underbrace{\Pi(x) \dots * \Pi(x)}_{n \text{ times}}. \quad (2)$$

The rectangular function $\Pi(x)$ equals 1 for $|x| \leq \frac{1}{2}$ and 0 else. The support of the 2-D splines equals $[-(n+1)/2, (n+1)/2] \times [-(n+1)/2, (n+1)/2]$. Due to the compact support of splines, the hybrid shift-invariant spaces $V(\mathcal{G})$ they induce are *not* band-limited and highly *local* in the sense that according to $h(x, y; t) = \sum_{m=1}^M \sum_{(k,l) \in \mathbb{A}_m} c_{k,l}(t) b_{n(m)}(x-k, y-l)$ the field value $h(x, y; t)$ at any given position $(x_0, y_0) \in \mathcal{A}$ depends on at most $(N+1)^2$ coefficients (here, $N = \max\{n(m)\}_{m=1, \dots, M}$ denotes the largest spline order occurring in \mathcal{G}).

3.3. Time-varying Non-wave Fields

The physical fields monitored by a WSN are usually governed by differential equations and rarely are band-limited. We briefly verify the suitability of hybrid shift-invariant spaces as field models by considering diffusion fields, an example of which is shown in the upper part of Fig. 1. Consider P sources whose strength, position, and activation time are denoted by A_p , (x_p, y_p) , and t_p , respectively. The resulting 2-D diffusion field can then be written as

$$h(x, y; t) = \sum_{p=1}^P A_p K(x - x_p, y - y_p; t - t_p) \quad (3)$$

with the heat kernel

$$K(x, y; t) = H(t) \frac{1}{4\pi\kappa t} e^{-\frac{x^2+y^2}{4\pi\kappa t}}. \quad (4)$$

Here, $H(t)$ denotes the unit step function which equals 1 for $t \geq 0$ and 0 for $t < 0$, and κ is the diffusion coefficient (e.g., thermal conductivity in the case of a temperature field). In the simulations section, we will exclusively use diffusion fields given by (3).

4. RECONSTRUCTION OF TIME-VARYING FIELDS

4.1. Reconstruction Problem

The field reconstruction method described below is an extension of [10] to 2-D hybrid shift-invariant spaces. Our aim is to reconstruct the spatial field $h(x, y; nT)$ at the sampling instants from the sensor measurements $h_i(n)$. This amounts to finding an estimate $\hat{h}(x, y; nT) \in V(\mathcal{G})$, or equivalently, to determining coefficient estimates $\hat{c}_{k,l}(nT)$. With our assumption of spline generators, the localized nature of $V(\mathcal{G})$ implies that the coefficients $\hat{c}_{k,l}(nT)$ can be computed separately for any subset \mathbb{A}_m . Consequently, all cluster-heads can perform local field reconstruction independently of each other. Hence, in the following we will only consider reconstruction within one sub-region \mathcal{A}_m , associated to the cluster \mathcal{C}_m which consists of $I_m = |\mathcal{C}_m|$ sensors.

Denoting the maximum spline order in \mathcal{G} by N , any field value $h(x', y'; nT)$ is completely determined by the coefficients $c_{k,l}(nT)$ in the neighborhood $(x', y') + \mathcal{S}$ with $\mathcal{S} \triangleq [-(N+1)/2, (N+1)/2] \times [-(N+1)/2, (N+1)/2]$. Thus, reconstruction within \mathcal{A}_m requires only the $J_m \triangleq |\mathbb{Z}_m^2|$ coefficients $c_{k,l}(nT)$ lying within $\mathcal{A}_m + \mathcal{S}$, i.e., for $(k, l) \in \mathbb{Z}_m^2 \triangleq \mathbb{Z}^2 \cap (\mathcal{A}_m + \mathcal{S})$. Correspondingly, least-squares field reconstruction amounts to minimizing

$$\sum_{i \in \mathcal{C}_m} \left| \sum_{(k,l) \in \mathbb{Z}_m^2} c_{k,l}(nT) b_{n(k,l)}(x_i - k, y_i - l) - h_i(nT) \right|^2 \quad (5)$$

with respect to $c_{k,l}(nT)$, $(k, l) \in \mathbb{Z}_m^2$. Here, $n(k, l)$ is the spline order associated to (k, l) . To obtain a reformulation of the field reconstruction in terms of matrices and vectors we arrange the sensor measurements and unknown coefficients into respective vectors $\mathbf{h}(n)$ and $\mathbf{c}(n)$ according to

$$[\mathbf{h}(n)]_j = h_{i_j}(n), [\mathbf{c}(n)]_r = c_{k_r, l_r}(nT), \quad (6)$$

and we define the $I_m \times J_m$ matrix

$$[\mathbf{G}]_{j,r} = b_{n(k_r, l_r)}(x_{i_j} - k_r, y_{i_j} - l_r). \quad (7)$$

Here, i_j , $j = 1, \dots, I_m$, denotes the indices of the sensors located in \mathcal{A}_m and $\{(k_r, l_r)\}_{r=1, \dots, J_m}$ denotes the J_m index pairs in \mathbb{Z}_m^2 arranged into a list. Using these definitions we rewrite the LS minimization problem (5) as

$$\hat{\mathbf{c}}(n) = \arg \min_{\mathbf{c}} \|\mathbf{G}\mathbf{c} - \mathbf{h}(n)\|^2. \quad (8)$$

Once the optimum coefficients $\hat{c}_{k,l}(n)$ have been computed, the field within \mathcal{A}_m can be reconstructed as

$$\hat{h}(x, y; nT) = \sum_{k, l \in \mathbb{Z}_m^2} \hat{c}_{k,l}(nT) b_{n(k, l)}(x - k, y - l), \quad (x, y) \in \mathcal{A}_m. \quad (9)$$

4.2. Solution

The problem (8) amounts to having the cluster head solve the associated normal equations

$$\mathbf{G}^H \mathbf{G} \hat{\mathbf{c}}(n) = \mathbf{G}^H \mathbf{h}(n). \quad (10)$$

which leads to

$$\hat{\mathbf{c}}(n) = \mathbf{G}^\# \mathbf{h}(n) \quad \text{with } \mathbf{G}^\# = (\mathbf{G}^H \mathbf{G})^{-1} \mathbf{G}^H. \quad (11)$$

In order for this solution to exist, the matrix \mathbf{G} must have full rank, which in turn requires that there are sufficiently many sensors (at least as many as unknown coefficients) appropriately placed to sample the field. Technically, the sensor positions $\{(x_i, y_i)\}_{i \in \mathcal{C}_m}$, have to form a so-called stable sampling set (see [10]). For the one-dimensional case, stable sampling sets for B-spline spaces are well understood. This is not true for the 2-D case, where only probabilistic statements have been obtained [11].

The compact support of the spline generators implies that the matrix \mathbf{G} is sparse, where the degree of sparsity depends on the size of \mathcal{A}_m and on the spline order. Indeed, $b_{n(k_r, l_r)}(x_{i_j} - k_r, y_{i_j} - l_r) = 0$ if $|x_{i_j} - k_r| > (n(k_r, l_r) + 1)/2$ or $|y_{i_j} - l_r| > (n(k_r, l_r) + 1)/2$, and thus at most $(n(k_r, l_r) + 1)^2 \leq (N + 1)^2$ of the J_m elements in each row can be non-zero. Furthermore, the Gram matrix $\mathbf{G}^H \mathbf{G}$ partly inherits the sparsity of \mathbf{G} . In order to keep memory and complexity as low as possible, a solver for (10) should capitalize on the sparsity of the matrices involved. Efficient direct (i.e., non-iterative) solvers based on the Cholesky factorization $\mathbf{G}^H \mathbf{G} = \mathbf{C} \mathbf{C}^H$ of the Gramian (here, \mathbf{C} is a $J_m \times J_m$ lower triangular matrix) [12] followed by forward elimination and backward substitution have been discussed in [1, 2].

4.3. Iterative Solvers for the LS Problem

With direct methods it may sometimes be difficult to exploit the sparsity of \mathbf{G} . In contrast, iterative methods, which generate a sequence of refined approximate solutions $\hat{\mathbf{c}}^{(q)}(n)$, $q = 1, 2, 3, \dots$, usually only involve simple matrix-vector multiplications in which the sparsity of \mathbf{G} can be directly exploited. Furthermore, in our time-varying

context, the iterative solvers can be initialized at time n with the solution $\hat{\mathbf{c}}(n-1)$ obtained in the previous time-slot. Such an initialization can significantly reduce the number of iterations, provided the field coefficients change only moderately, as can be expected e.g. for the diffusion field model (3). With iterative solvers, the iterations are terminated either when a certain accuracy has been achieved or a prescribed maximum number of iterations is reached. The latter has a regularizing effect which is desirable for highly irregular sensor placements and noisy field measurements.

An effective iterative method for solving symmetric positive definite linear equations such as (10) is preconditioned conjugate gradient [12] and its variants like MINRES [13], GMRES [14], and LSQR [15]. We prefer LSQR in our setup since it can operate directly on the rectangular least-squares problem and avoids the computation of the Gram matrix (which would implicitly square the condition number).

4.4. Algorithm Summary and Complexity

In the following, we summarize all algorithmic steps necessary to perform iterative field reconstruction and we provide estimates for their computational complexity.

Preprocessing. With the LSQR solver, the only preprocessing to be performed by the cluster-head is the computation of \mathbf{G} according to (7). This can be done during the initialization phase of the WSN, as soon as the sensors have provided their position information but before any measurements $h_i(n)$ are obtained. The complexity of this step is given by $\mathcal{O}(I_m(N+1)^2)$ function evaluations.

Coefficient Estimation. Using the LSQR solver mainly amounts to repeated application of \mathbf{G} and \mathbf{G}^H to certain intermediate vectors, resulting in an overall complexity of $\mathcal{O}(I_m(N+1)^2)$ operations per iteration.

Field Reconstruction. Finally, the field can be reconstructed for any point $(x, y) \in \mathcal{A}_m$ according to (9). This requires $\mathcal{O}((N+1)^2)$ operations per spatial point.

We emphasize that the complexity of all steps scales only *linearly* with the number of sensors. The coefficient estimation and field reconstruction have to be performed during each time slot. Since the number of LSQR iterations on average can be kept low by the proposed initialization, the overall complexity of our field reconstruction scheme is extremely low. In order to keep the communication requirements low and distribute the computational effort evenly, many small clusters appear desirable. However, a small cluster size tends to deteriorate the condition number of \mathbf{G} since the assumption $I_m \geq J_m$ will be violated more often; in such cases, the reconstruction may be locally poor or fail completely.

5. IMPACT OF SENSOR LOCALIZATION ERRORS

We have previously studied the impact of measurement and quantization noise in [1, 2]. Here, we investigate the impact of sensor localization errors in the absence of other impairments, focusing for simplicity on the one-dimensional (1-D) case. While the actual sensor positions equal \tilde{x}_i , the sensors report estimated positions x_i to the cluster-heads. Due to localization errors, x_i differs from \tilde{x}_i . We denote by $\delta_i = \tilde{x}_i - x_i$ the localization errors which are assumed to be i.i.d. uniform between $-\Delta_0$ and Δ_0 . For notational convenience, we further drop the time index n and the cluster index m and assume that the actual field is given by $h(x) = \mathbf{c}^T \mathbf{g}(x)$ where $\mathbf{g}(x) = (g(x - k))_{k \in \mathcal{A} \cap \mathbb{Z}}^T$ and \mathbf{c} is the vector with the true field coefficients which are assumed to be i.i.d. with zero mean and variance

σ_c^2 . The reconstructed field is given by $\hat{h}(x) = \hat{\mathbf{c}}^T \mathbf{g}(x)$ where $\hat{\mathbf{c}}$ denotes the coefficients estimated according to (the 1-D version of) (11) with the the measurements given by $\tilde{h}_i = h(\tilde{x}_i) = h(x_i + \delta_i)$. Clearly, sensor localization errors cause a mismatch between the sensor positions and the sensor measurements used for the reconstruction. The mean-square reconstruction error within \mathcal{A} can now be developed as

$$\begin{aligned} \text{MSE} &= E \left\{ \int_{\mathcal{A}} (\hat{h}(x) - h(x))^2 dx \right\} = E \left\{ \int_{\mathcal{A}} ((\hat{\mathbf{c}} - \mathbf{c})^T \mathbf{g}(x))^2 dx \right\} \\ &= \int_{\mathcal{A}} \mathbf{g}^T(x) E \{ (\hat{\mathbf{c}} - \mathbf{c})(\hat{\mathbf{c}} - \mathbf{c})^T \} \mathbf{g}(x) dx = \text{tr}\{\mathbf{C}_{\hat{\mathbf{c}}-\mathbf{c}} \mathbf{G}_{\mathbf{g}}\}, \end{aligned}$$

where the expectation is with respect to the localization errors δ_i and the field coefficients \mathbf{c} . In the last expression, we introduced the Gramian $\mathbf{G}_{\mathbf{g}} = \int_{\mathcal{A}} \mathbf{g}(x) \mathbf{g}^T(x) dx$ and the matrix $\mathbf{C}_{\hat{\mathbf{c}}-\mathbf{c}} = E \{ (\hat{\mathbf{c}} - \mathbf{c})(\hat{\mathbf{c}} - \mathbf{c})^T \}$ which is the correlation matrix of the coefficient errors $\hat{\mathbf{c}} - \mathbf{c}$. The Gramian $\mathbf{G}_{\mathbf{g}}$ can easily be shown to be a symmetric banded Toeplitz matrix (the band structure results from the compact support of the B-spline generators). Since the coefficient error can be written as (cf. (11))

$$\hat{\mathbf{c}} - \mathbf{c} = \mathbf{G}^\# \tilde{\mathbf{h}} - \mathbf{G}^\# \mathbf{h} = \mathbf{G}^\# \mathbf{e} \quad \text{with } \mathbf{e} = \tilde{\mathbf{h}} - \mathbf{h},$$

its correlation matrix equals

$$\mathbf{C}_{\hat{\mathbf{c}}-\mathbf{c}} = \mathbf{G}^\# \mathbf{C}_{\mathbf{e}} (\mathbf{G}^\#)^T, \quad \text{where } \mathbf{C}_{\mathbf{e}} = E \{ \mathbf{e} \mathbf{e}^T \}.$$

The element e_i of \mathbf{e} , i.e., the measurement error at sensor i caused by the localization error δ_i , reads

$$e_i = \tilde{h}_i - h_i = \sum_k c_k \Delta_g(x_i - k, \delta_i),$$

where $\Delta_g(x, \delta) = g(x + \delta) - g(x)$. Using the independence of the field coefficients c_k and of the localization error δ_i , it follows that the (i, j) th element of $\mathbf{C}_{\mathbf{e}}$ equals

$$E\{e_i e_j\} = \begin{cases} \sigma_c^2 \sum_k E\{\Delta_g^2(x_i - k, \delta_i)\}, & i=j, \\ \sigma_c^2 \sum_k E\{\Delta_g(x_i - k, \delta_i)\} E\{\Delta_g(x_j - k, \delta_j)\}, & i \neq j, \end{cases}$$

where the expectations now is with respect to δ_i only. The above expressions can be specialized to any spline generator $g(x) = \tilde{b}_n(x)$. For reasons of space, we only provide the results for $n = 1$, i.e.,

$$\tilde{b}_1(x) = \begin{cases} 1 - |x|, & |x| \leq 1, \\ 0, & \text{else.} \end{cases}$$

Here, the first row of the symmetric Toeplitz matrix \mathbf{G}_g equals $(\frac{4}{9} \frac{1}{6} 0 \dots 0)$. Furthermore, denoting the integer closest to x_i by k_i and the distance of x_i from the closest integer by $\bar{x}_i = k_i - x_i$, the (normalized) variance of the field measurement error is obtained as

$$\frac{E\{e_i^2\}}{\sigma_c^2} = \begin{cases} \frac{2\Delta_0^2}{3} & |\bar{x}_i| \geq \Delta_0, \\ \frac{2\Delta_0^2}{3} - \frac{3\Delta_0|\bar{x}_i|}{2} + 3\bar{x}_i^2 - \frac{3|\bar{x}_i|^3}{2\Delta_0} & |\bar{x}_i| < \Delta_0. \end{cases}$$

The correlations equal $E\{e_i e_j\} = \rho_{ij} \sigma_c^2 p(\bar{x}_i) p(\bar{x}_j)$, where

$$p(z) = \begin{cases} \frac{z^2}{4\Delta_0} - \frac{|z|}{2} + \frac{\Delta_0}{4} & |z| < \Delta_0, \\ 0 & \text{else,} \end{cases}$$

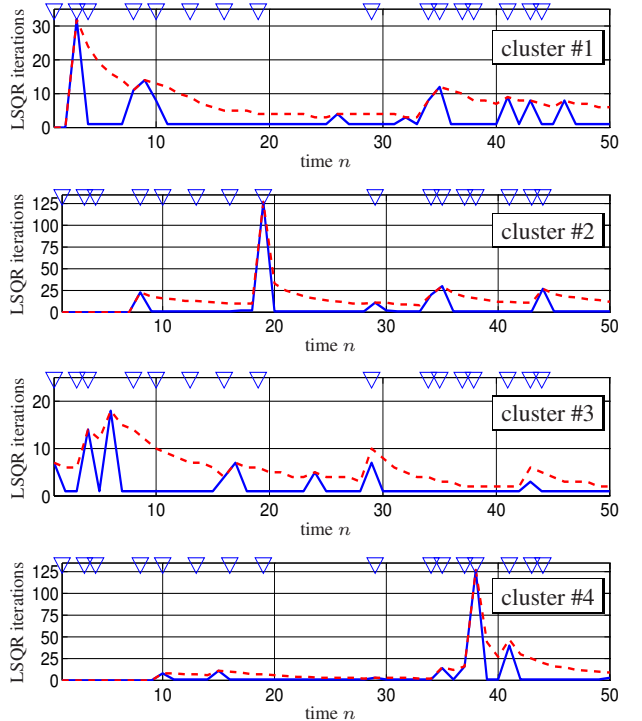


Fig. 2. Number of LSQR iterations required to obtain a normalized square error of -10 dB versus time n for each of the four clusters. Solid blue lines correspond to proposed LSQR initialization and dashed red lines correspond to standard LSQR initialization.

and the coefficients ρ_{ij} are given by

$$\rho_{ij} = \begin{cases} 6, & k_i = k_j, \\ -4, & |k_i - k_j| = 1, \\ 1, & |k_i - k_j| = 2, \\ 0, & |k_i - k_j| \geq 3. \end{cases}$$

6. NUMERICAL SIMULATIONS

6.1. Iterative Reconstruction of Time-Varying Fields

We illustrate the performance of the iterative reconstruction algorithm for a time-varying diffusion field using LSQR. The diffusion fields were constructed according to (3), with $P = 16$ sources activated at Poisson distributed time instants t_p over the interval $[0, 50T]$, the source positions (x_p, y_p) uniformly distributed over \mathcal{A} , and the amplitudes A_p uniformly distributed over the interval $[-10, 10]$. The WSN consisted of $I = 30^2 = 900$ sensors deployed on a square grid over a square region $\mathcal{A} = [0, 20] \times [0, 20]$. The overall region was split into $M = 4$ disjoint square subregions \mathcal{A}_m of identical size (see Fig. 1), each corresponding to one sensor cluster with $I_m = 225$ sensors. For the reconstruction, we used spline generators whose order was empirically optimized within each cluster. The field estimates obtained by the individual clusters were super-imposed using weight functions $w_m(x, y)$ in order to obtain smooth transitions at the cluster boundaries. The weight functions are designed to satisfy $\sum_{m=1}^M w_m(x, y) = 1$ (Fig. 1 shows an example of the weight function for $m = 1$). We measured the reconstruction quality in terms of the normalized square error

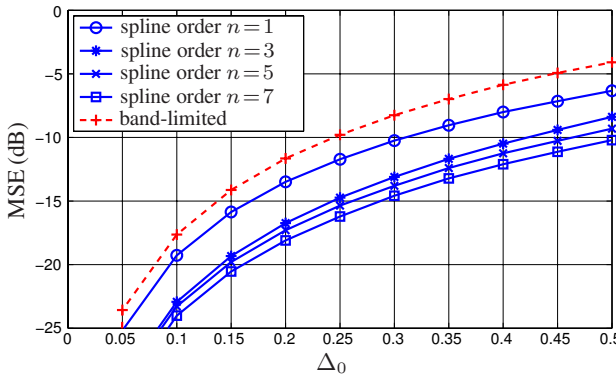


Fig. 3. Mean square error (MSE) versus maximal localization error Δ_0 for field reconstruction using spline orders $n \in \{1, 3, 5, 7\}$ and sinc-type generator functions (band-limited reconstruction).

between $\hat{h}(x, y; nT)$ and $h(x, y; nT)$. Fig. 2 shows for each of the four clusters the number of LSQR iterations¹ required to obtain a normalized squared error of -10 dB. We compare LSQR with the standard initialization (an all-zero vector) and LSQR initialized using the field coefficients estimated in the previous time-slot. The activation times of the sources are marked with ∇ at the top of each plot. It can be seen that, as expected, the proposed initialization indeed leads to a significantly smaller number of iterations than with the standard initialization. Furthermore, the number of LSQR iterations is quite small most of the time. Only if a source becomes active in a given cluster and the field changes noticeable, then the corresponding cluster-head needs to perform a larger number of iterations. Note that source activation mostly affects only a single cluster, e.g., at time $n = 19$ a source becomes active in cluster #2 and only the corresponding cluster-head has increased workload whereas the other cluster-heads need to perform only very few updates at this time instant to track the diffusion process. We finally note that there are some small peaks in the iteration count even when no source becomes active (e.g., at $n = 26$ in cluster #1); this can be attributed to field changes that occur when a previously activated source starts to diffuse across a cluster boundary.

6.2. Localization Error

We compare the impact of uniformly distributed localization errors on the reconstruction quality for different spline orders and for BL reconstruction. We constructed fields belonging to shift-invariant spaces with different spline orders according to (1). The field coefficients $c_{k,l}$ that were uniformly distributed in the interval $[-10, 10]$. Field reconstruction was performed using the correct spline order (therefore avoiding a systematic mismatch) but incorrect sensor positions. Thus, the localization error was the only source of error. The sensors were deployed regularly on the integer lattice (at critical density). The localization errors were uniform in the interval $[-\Delta_0, \Delta_0]$ with Δ_0 ranging from 0 to 0.5. Fig. 3 shows the MSE obtained for different splines orders versus the maximal localization error Δ_0 . It is seen that all spline reconstructions are less sensitive to localization errors than BL reconstruction. In this scenario, spline order $n = 0$ (not shown) is actually completely insensitive against sensor localization errors (i.e., there is no reconstruction error). For $n > 0$, the reconstruction MSE decreases with increasing order, i.e.,

¹We note that before the first source becomes active, the sensor measurements are all zero and therefore no reconstruction is performed, in which case the number of iterations equals 0.

large spline orders are less sensitive to localization errors. This can be attributed to the fact that the spline curvature about the origin is smaller for larger spline order.

7. CONCLUSIONS

We studied a clustered sensor network architecture for reconstructing and tracking time-varying non-bandlimited fields that is based on the concept of hybrid shift-invariant spaces with B-splines as generator functions. To solve the underlying least-squares problem, we proposed to use iterative algorithm like LSQR which are initialized using the field coefficient estimates from the previous time slot. Furthermore, we analytically and numerically investigated the sensitivity of our scheme to sensor localization errors. Our scheme features excellent reconstruction quality, is less sensitive to localization errors than BL reconstruction, requires little communication overhead, and has extremely low computational complexity (a small number of LSQR iterations each of which scales linearly with the number of sensors).

REFERENCES

- [1] G. Reise and G. Matz, "Distributed sampling and reconstruction of non-bandlimited fields in sensor networks based on shift invariant spaces," in *Proc. ICASSP 2009*, Taipeh, Taiwan, April 2009, pp. 2061–2064.
- [2] G. Reise and G. Matz, "Clustered wireless sensor networks for robust distributed field reconstruction based on hybrid shift-invariant spaces," in *Proc. SPAWC 2009*, Perugia, Italy, Jun. 2009, pp. 66–70.
- [3] A. Aldroubi and K. Gröchenig, "Nonuniform sampling and reconstruction in shift-invariant spaces," *SIAM Review*, vol. 43, no. 4, pp. 585–620, 2001.
- [4] P. Ishwar, A. Kumar, and K. Ramchandran, "Distributed sampling in dense sensor networks: a 'bit-conservation principle,'" in *Proc. IEEE Int. Symp. Information Processing in Sensor Networks*, Palo Alto, CA, Apr. 2003, pp. 17–31.
- [5] A. Nordio, C. F. Chiasseroni, and E. Viterbo, "Performance of linear field reconstruction techniques with noise and uncertain sensor locations," *IEEE Trans. Signal Processing*, vol. 56, no. 9, pp. 3535–3547, Aug. 2008.
- [6] A. Kumar, P. Ishwar, and K. Ramchandran, "On distributed sampling of smooth non-bandlimited fields," in *Proc. IEEE Int. Symp. Information Processing in Sensor Networks*, Berkeley, CA, Apr. 2004, pp. 89–98.
- [7] F. S. Cattivelli, C. G. Lopes, and A. H. Sayed, "Diffusion recursive least-squares for distributed estimation over adaptive networks," *IEEE Trans. Signal Processing*, vol. 56, no. 5, pp. 1865–1877, Jan. 2008.
- [8] G. Mao, B. Fidan, and B. D. O. Anderson, "Wireless sensor network localization techniques," *Computer Networks: The International Journal of Computer and Telecommunications Networking*, vol. 51, no. 10, pp. 2529–2553, 2007.
- [9] Q. Sun, "Frames in spaces with finite rate of innovation," *Advances in Computational Mathematics*, vol. 28, no. 301–329, 2008.
- [10] K. Gröchenig and H. Schwab, "Fast local reconstruction methods for nonuniform sampling in shift-invariant spaces," *SIAM J. Matrix Anal. Appl.*, vol. 24, no. 4, pp. 899–913, April 2003.
- [11] K. Gröchenig and R. F. Bass, "Random sampling of entire functions of exponential type in several variables," arXiv:0706.3818v2, 2008.
- [12] G.H. Golub and C.F. Van Loan, *Matrix Computations*, Johns Hopkins University Press, 3 edition, 1996.
- [13] C. C. Paige and M. A. Saunders, "Solution of sparse indefinite systems of linear equations," *SIAM J. Numer. Anal.*, vol. 12, no. 4, pp. 617–629, 1975.
- [14] Y. Saad and M. Schultz, "GMRES: A generalized minimal residual algorithm for solving nonsymmetric linear systems," *SIAM J. Sci. Stat. Comput.*, vol. 7, no. 3, pp. 856–869, July 1986.
- [15] C. C. Paige and M. A. Saunders, "LSQR: An algorithm for sparse linear equations and sparse least squares," *ACM Trans. on Mathematical Software*, vol. 8, no. 1, pp. 43–71, Mar. 1982.